Supplement of Atmos. Chem. Phys., 20, 13069–13089, 2020
https://doi.org/10.5194/acp-20-13069-2020-supplement

Atmospheric Chemistry and Physics
Open Access
EGU

Supplement of

Role of the dew water on the ground surface in HONO distribution: a case measurement in Melpitz

Yangang Ren et al.

Correspondence to: Abdelwahid Mellouki (abdelwahid.mellouki@cnrs-orleans.fr) and Hartmut Herrmann (herrmann@tropos.de)

Intercomparison strategy:

To improve the understanding of the chosen intercomparison setup, we refer to the Fig. S1. In Fig. S1b, the MARGA PM_{10} inlet is shown. This inlet was used to for both instruments in the first measurement period to identify the inlet artifact. Therefore, the inlet tube was extended with a Y-connector (Fig. S1a) within the measurement container. The tube from the inlet to the connector had a length of approximately 2 m.

For the second intercomparison period the LOPAP inlet was set next to the MARGA inlet on the roof of the container. No interactions between LOPAP and MARGA inlet occurred.

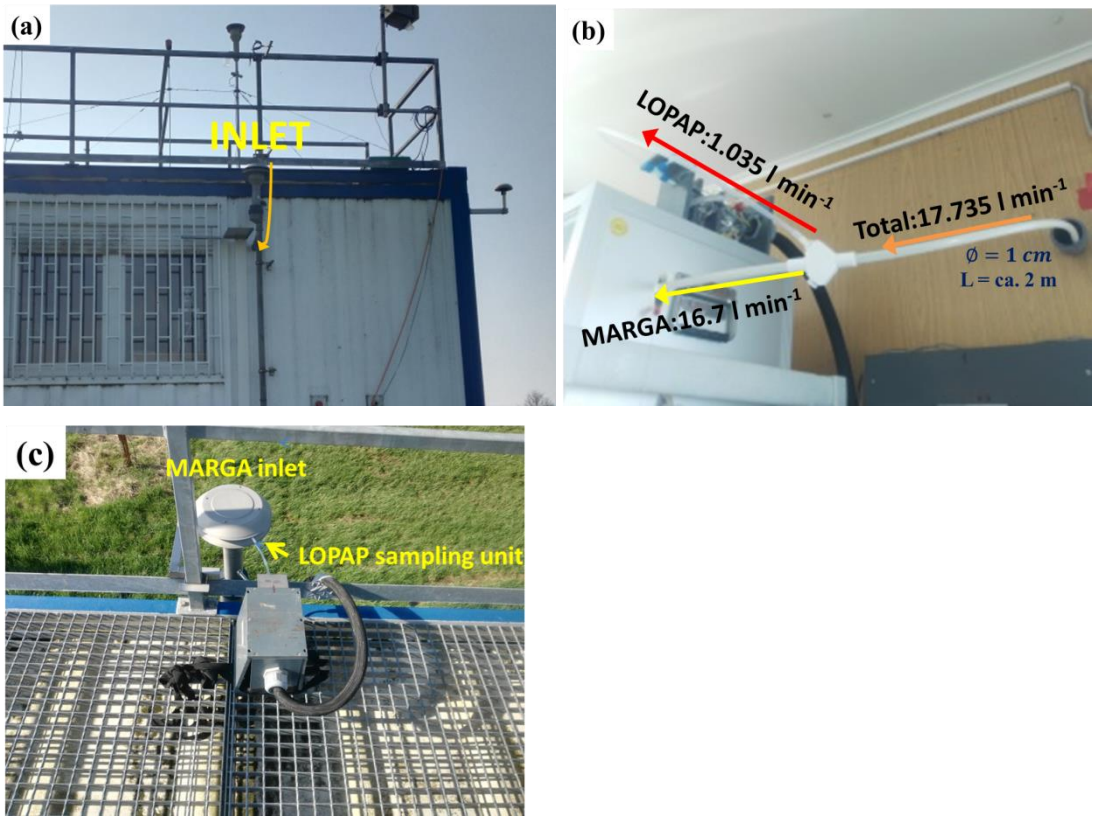

Fig. S1. (a) the sampling inlet of LOPAP and MARGA; (b) M1; sampling unit of LOPAP was connected in front of the WRD and in the back of the 2 m sampling inlet of MARGA (April 18th, 2018 13:00 UTC –April 20th, 2018 08:00 UTC); (c) M2; sampling unit of LOPAP was settled in the same level as the sampling head of MARGA (April 20th, 2018 15:00 UTC – April 29th, 2018 07:00 UTC).

Fig. S2. The dew collector system: The glass sampler surface is 1.0×1.5 m^2, and about 40 cm above ground at the lowest point.

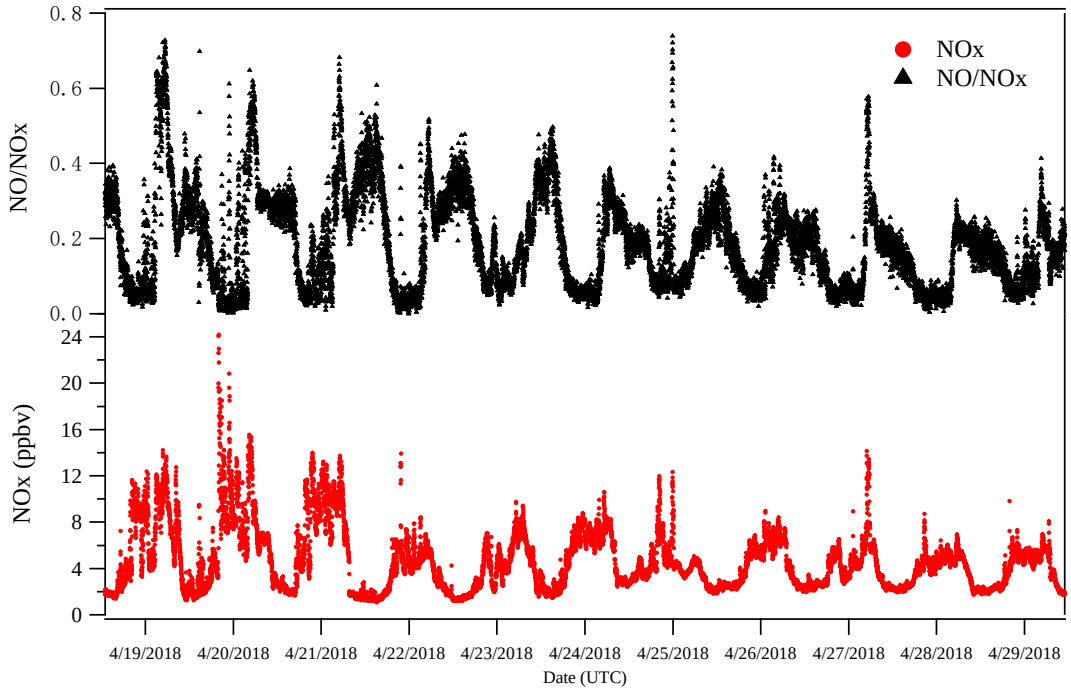

Fig. S3. Time profile of NO_x and NO/NO_x from April 19th to 29th, 2018.

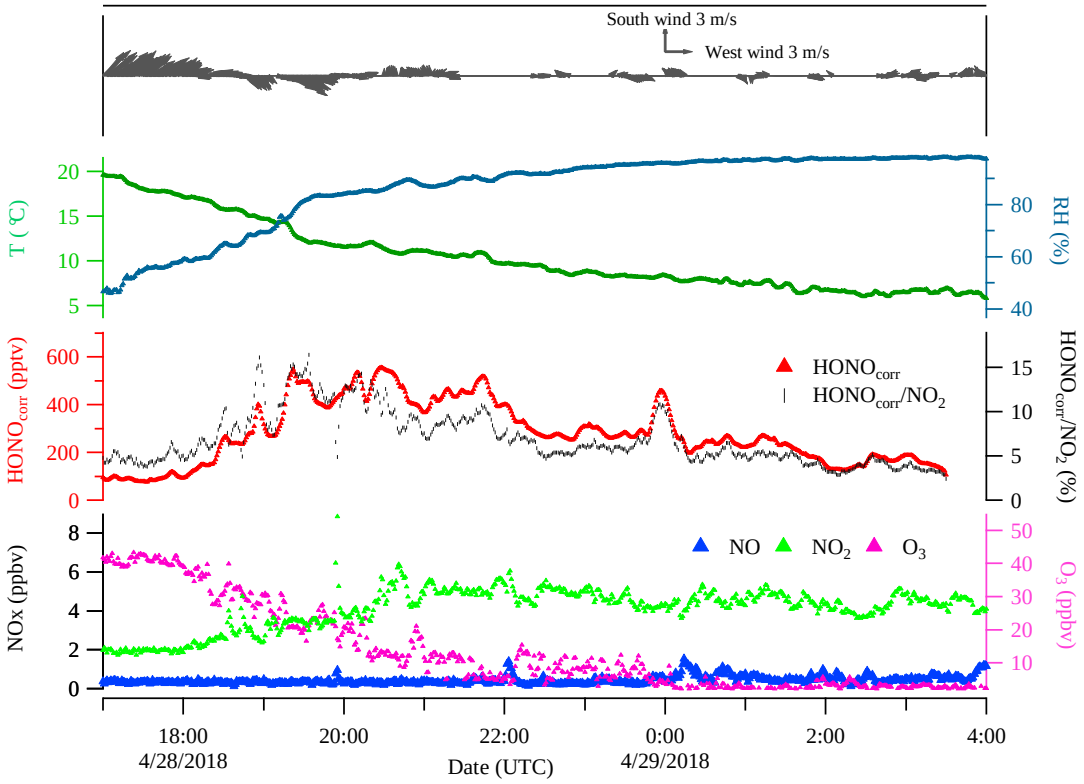

Fig. S4. A case of the determination of the heterogeneous NO_2-to-HONO conversion frequency at night from April 28th until April 29th 2018.

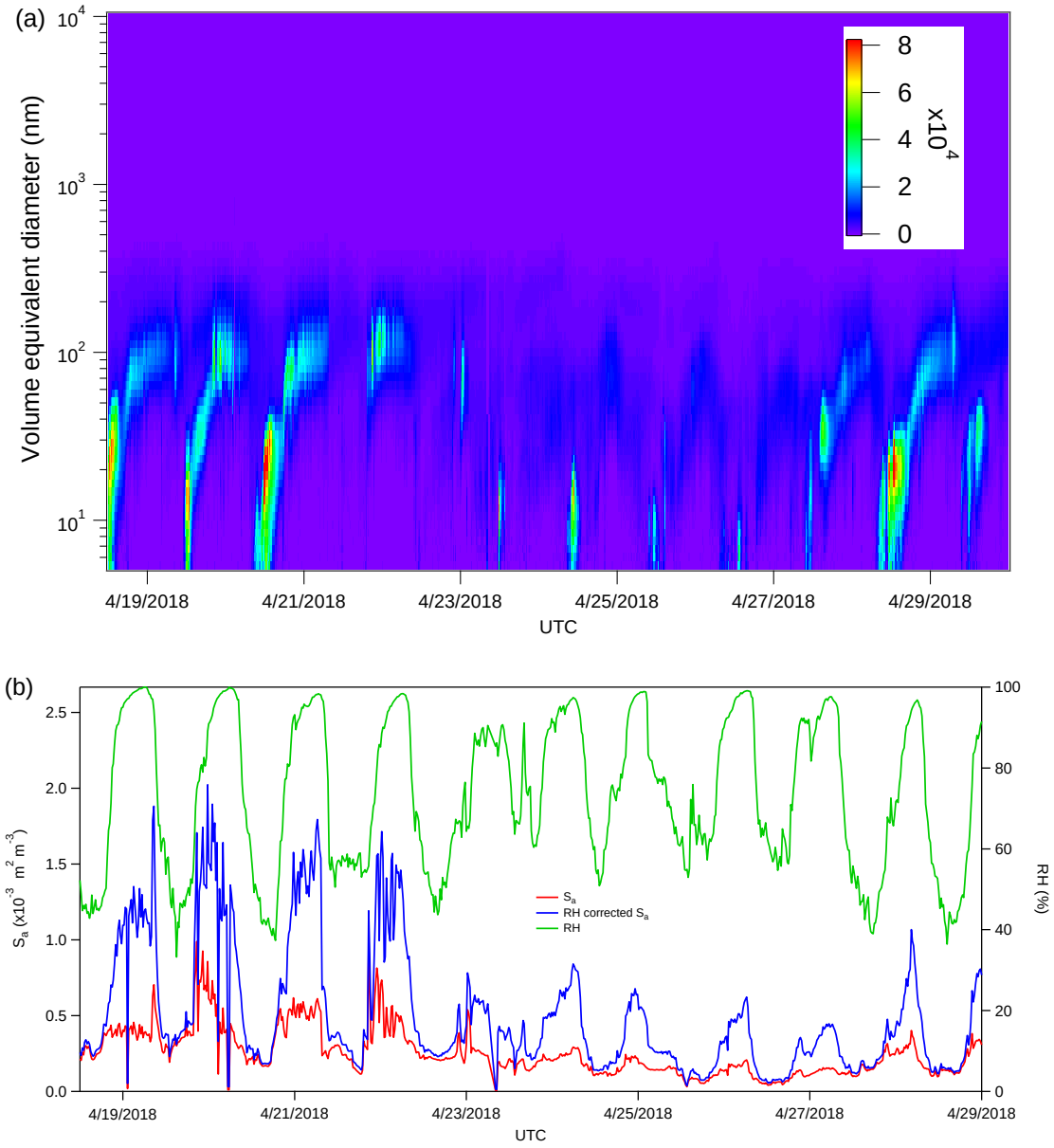

Fig. S5. (a) Particle size distribution ranged from 5 nm to 10 μm of APSS and D-MPSS data. The mobility diameter is to be assumed to be identical to the volume equivalent diameter due to compact particles. The color code presents the particle number density. (b) The particle surface density S_a and RH corrected S_a value calculated from the particle size distribution for our field measurement period of April 19th-29th 2018.

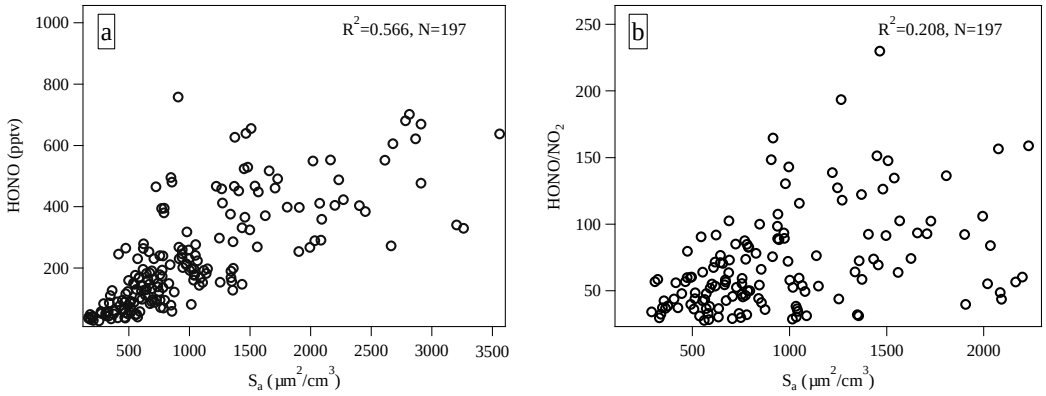

Fig. S6. Correlation between (a) $HONO_{corr}$ and (b) $HONO_{corr}/NO_2$ with particle surface density during the time interval of 17:30-22:00 (UTC) since the HONO concentration started to decrease from the midnight.

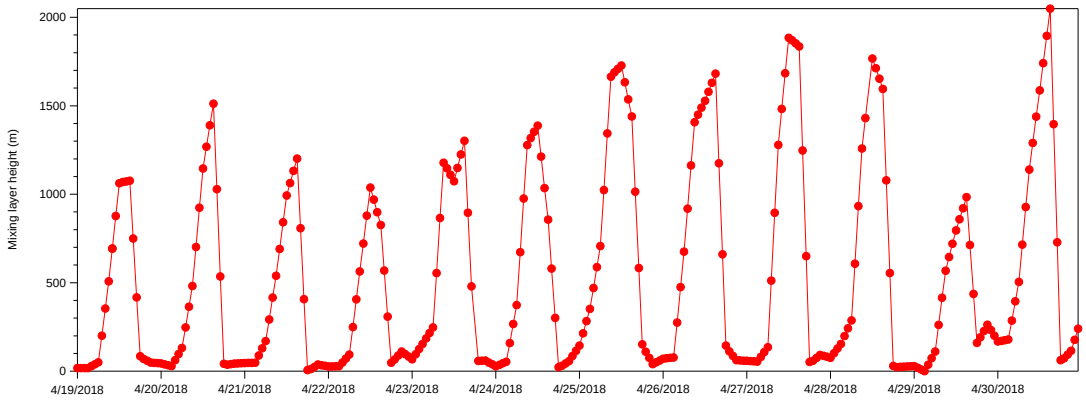

Fig. S7. Mixing layer height (H) in April 2018 calculated from the backward trajectory analysis based on GDAS data.

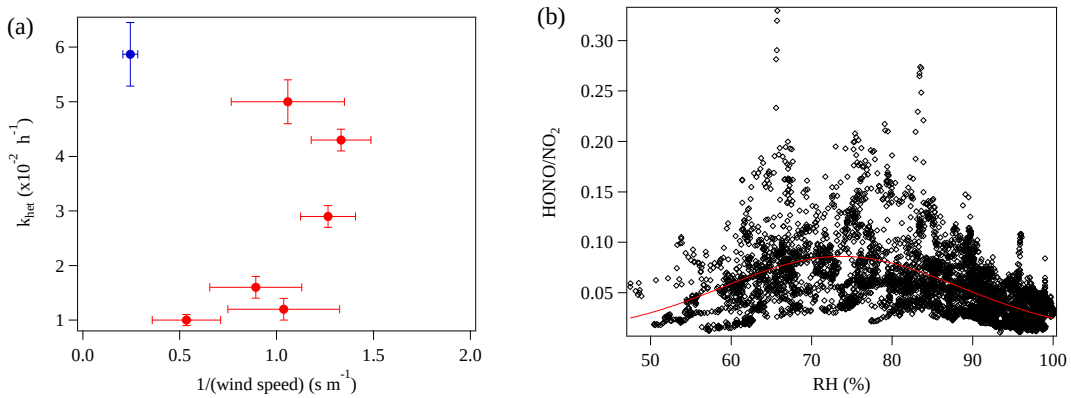

Fig. S8. Scatter plot of (a) NO_2-HONO conversion frequency (k_{het}) in Table 3 (in red) and also one data point (in blue) according to the second set of observation (mentioned in section 3.3 and Fig. 5) vs. the inverse of wind speed and (b) HONO/NO_2 against RH in the time interval of 18:00-04:00 (UTC) during the campaign period (April 19th to 29th, 2018).

Investigating resistance limitations in transport of HONO and NO_2 to the ground surface during the Melpitz measurement

In order to assess limitations of NO_2 conversion and HONO deposition in the surface parameterizations derived for the Melpitz dataset, a simple resistance model according to the description provided by Seinfeld and Pandis (2006), which has been proposed by Huff and Abbatt (2002) (Equation S1) was set up.

$$\upsilon_d = \frac{1}{R_a + R_b + R_c} \quad \text{(S1)}$$

Here, υ_d is the observed deposition velocity (cm s^{-1}), R_a is the aerodynamic transport resistance (Equation S2), R_b is the molecular diffusion resistance (Equation S3) and R_c is the reactive loss resistance (Equation S4). Each term can be calculated as follows

$$R_a = \left(\frac{1}{\mu\,\kappa^2}\right)\left[\ln\left(\frac{z}{z_0}\right)\right]^2 \quad \text{(S2)}$$

$$R_b = \frac{z_0}{D} \quad \text{(S3)}$$

$$R_c = \frac{4}{\gamma\, c} \quad \text{(S4)}$$

Where κ is the von Kármán constant (0.4) (VandenBoer et al., 2013), μ is the wind speed as 0.1 - 6 m s^{-1} in the pesent study, z_0 is an estimate of the roughness length of the surface (~ 0.03 m according to a 0.3 m grass height), z represents the surface layer height and is set to 15 m as example for nighttime values in Melpitz. Values for the local surface roughness length and surface layer height were approximated for atmospheric conditions with wind speeds less than 6 m s^{-1} (Huff and Abbatt, 2002;Seinfeld and Pandis, 2006). D is the molecular diffusivity of HONO and NO_2 as 5.7 $\times 10^{-5}$ and 1.5 $\times 10^{-5}$ m^2 s^{-1}, respectively, at 760 Torr (Hirokawa et al., 2008;Langenberg et al., 2019), γ is the reactive uptake coefficient and c is the mean molecular speed (~ 367 m s^{-1} for HONO and NO_2). These values were derived assuming that the upper limit to the observed HONO reactive uptake was limited equally by molecular diffusion and aerodynamic transport (Equation S1).

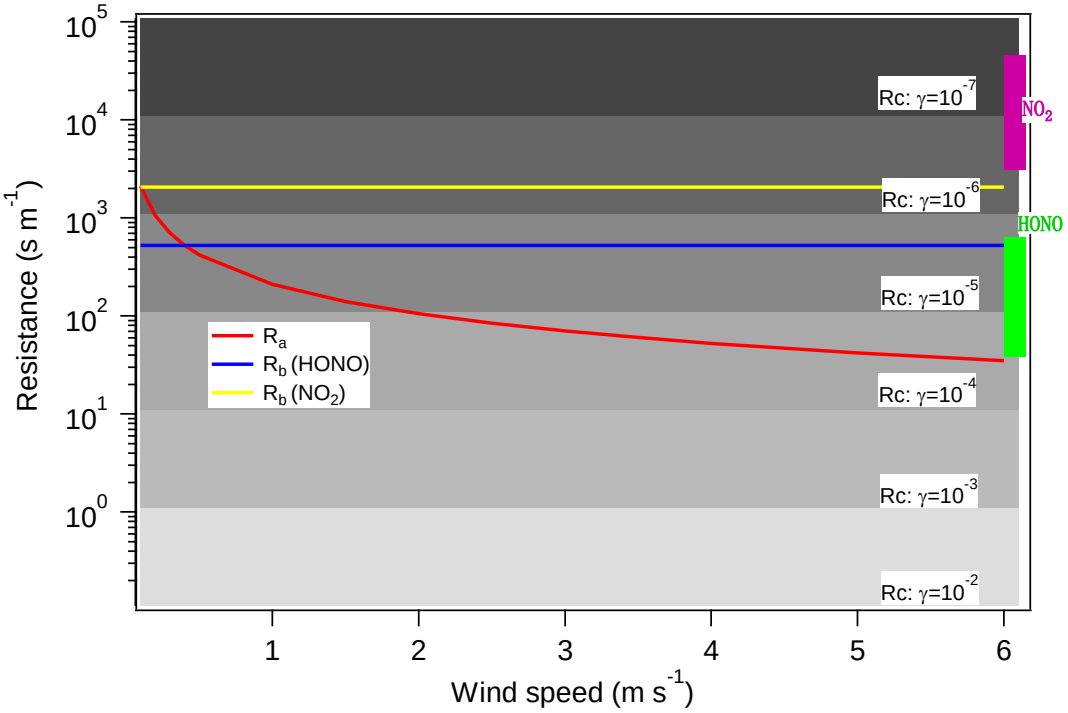

Fig. S9. Estimated contributions of resistance parameters to the observable ground surface processes for the HONO and NO_2 uptake values derived from Melpitz station. A series of grey shaded regions define the borders of the reactive uptake resistance (R_c), the R_c values calculated from upper and lower limit uptake values of HONO and NO_2 in this work are shown in green and pink column, respectively. The aerodynamic transport resistance (R_a, red line) and diffusion resistance (R_b, blue line for HONO and yellow for NO_2) are shown in the Figure."

Figure S9 shows the results of the calculated resistances using data limitations from the observation data set and compared to the observed range for HONO and NO_2 in Melpitz. This result presents that the aerodynamic transport resistance increases with decreasing windspeed and could play the main role for the HONO deposition when the wind speed was less than 0.5 m s^{-1}. Regarding on the calculated R_c range (region indicated by green bar) using the reactive uptake values observed for HONO (1.7×10^{-5} to 2.8×10^{-4}), limitation of the observed uptake of HONO was potentially significant from the molecular diffusion resistance term in the data range at wind speeds larger than ~1m s^{-1}. Therefore, the range of HONO uptake coeffcient values calculated in this investigation are potentially limited by a combination of both transport and diffusion to the ground surface. Since such limitations are realistic for the atmosphere, the γ-coefficients calculated here could have a broad scale applicability used for simulation of HONO production and loss at night when constrained by the observations. As shown in Fig. S9, the R_c range (region indicated by pink bar) calculated based on the reactive uptake values observed for NO_2 (2.4×10^{-7} to 3.5×10^{-6}) indicate limitation by the reactive

uptake process, which may play the main role rather than aerodynamic transport limitations and molecular diffusion limitations.

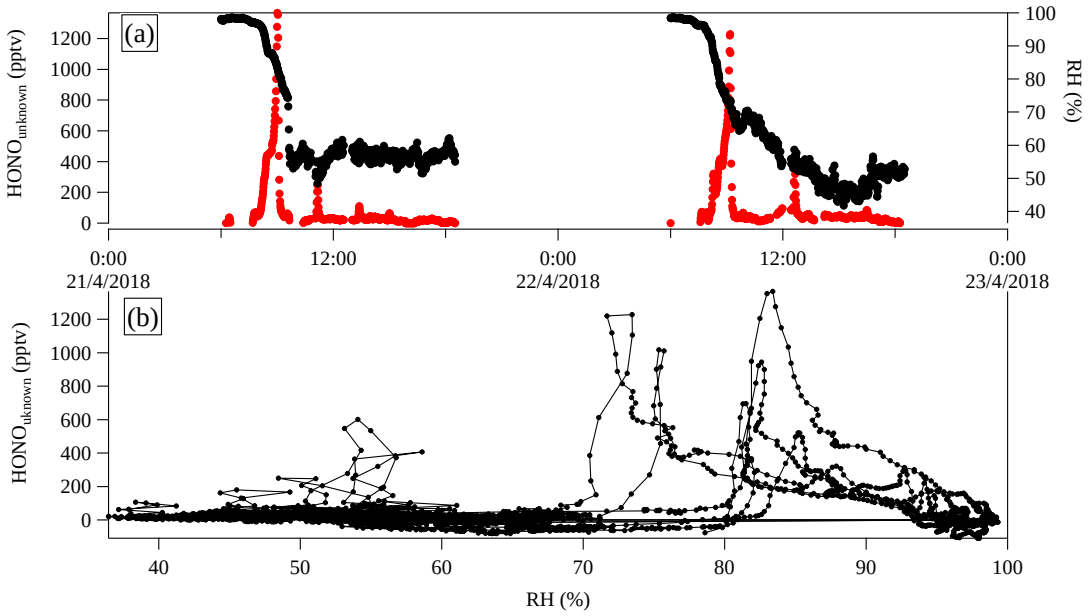

Fig. S10. (a) Example of time-profile of HONO and RH for the date April 21st to 22th to show that rapid humidity changes result in the release of HONO; (b) the HONO_unknown as a function of RH (%) during daytime in the period of April 20th to 29th, 2018; HONO_unknown was obtained by subtracting modeled HONO (HONO_Model4) from the measured HONO.

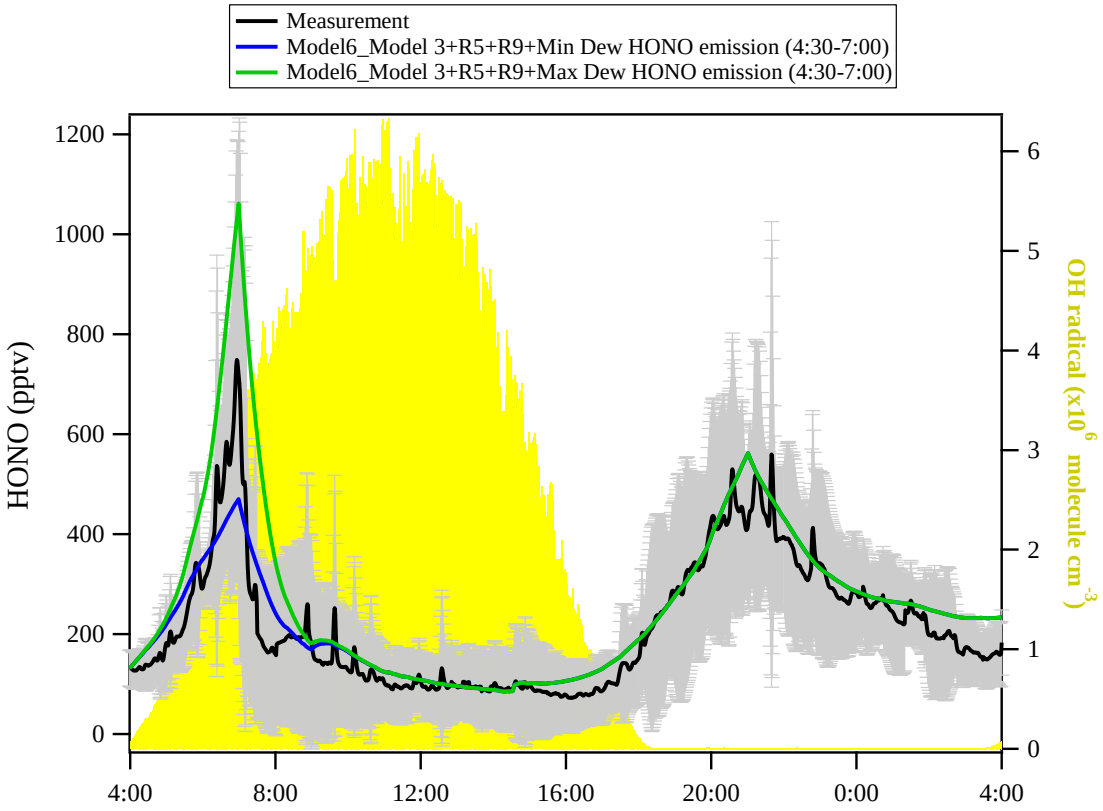

Fig. S11. Observed average HONO atmospheric concentration (black line, ±1σ in shaded area) and the calculated HONO concentration in model 6 using a min dew HONO emission $k_{emission}$ = 0.006 pptv $\%^{-1}$ s^{-1} (blue line) and max dew HONO emission $k_{emission}$ = 0.026 pptv $\%^{-1}$ s^{-1} (green line), respectively.

Reference

Hirokawa, J., Kato, T., and Mafuné, F.: Uptake of Gas-Phase Nitrous Acid by pH-Controlled Aqueous Solution Studied by a Wetted Wall Flow Tube, The Journal of Physical Chemistry A, 112, 12143-12150, 10.1021/jp8051483, 2008.

Huff, A. K., and Abbatt, J. P. D.: Kinetics and Product Yields in the Heterogeneous Reactions of HOBr with Ice Surfaces Containing NaBr and NaCl, The Journal of Physical Chemistry A, 106, 5279-5287, 10.1021/jp014296m, 2002.

Langenberg, S., Carstens, T., Hupperich, D., Schweighoefer, S., and Schurath, U.: Technical note: Determination of binary gas phase diffusion coefficients of unstable and adsorbing atmospheric trace gases at low temperature – Arrested Flow and Twin Tube method, Atmos. Chem. Phys. Discuss., 2019, 1-24, 10.5194/acp-2019-1050, 2019.

Seinfeld, J. H., and Pandis, S. N.: Atmospheric Chemistry and Physics: From Air Pollution to Climate Change, Wiley, 2006.

VandenBoer, T. C., Brown, S. S., Murphy, J. G., Keene, W. C., Young, C. J., Pszenny, A. A. P., Kim, S., Warneke, C., de Gouw, J. A., Maben, J. R., Wagner, N. L., Riedel, T. P., Thornton, J. A., Wolfe, D. E., Dubé, W. P., Öztürk, F., Brock, C. A., Grossberg, N., Lefer, B., Lerner, B., Middlebrook, A. M., and Roberts, J. M.: Understanding the role of the ground surface in HONO vertical structure: High resolution vertical profiles during NACHTT-11, J. Geophys. Res. Atmos., 118, 10,155-110,171, doi:10.1002/jgrd.50721, 2013.